19th International Conference
ENGINEERING MECHANICS 2013
Svratka, Czech Republic, May 13 – 16, 2013

ANALYSIS OF THE THERMAL BEHAVIOR OF MASS CONCRETE BASED ON SEMI-ADIABATIC TEMPERATURE MEASUREMENTS

W.R.L. Silva [1], V. Šmilauer [2], P. Štemberk [3]

Summary: *The combination of concrete's low thermal conductivity with exothermic hydration and ambient temperature leads to thermal gradients in concrete. Consequently, tensile stresses develop, leading to early age cracking that may compromise concrete durability. Hence, the prediction of mass concrete thermal behavior is necessary. Usually, this is done through FEM analysis in combination with adiabatic measurements of cement hydration. However, the use of adiabatic equipment is troublesome due to its high cost and lack of practicality. In that light, this work proposes a low-cost semi-adiabatic calorimeter setup. The measurements from this setup are used to adjust the parameters of an affinity hydration model. Next, the adjusted model is used as a basis for FEM thermal analyses of a mass concrete foundation block. Finally, the results from this analysis are compared against real scale measurements for validation.*

Keywords: ***adiabatic calorimeter, hydration, mass concrete***

1. Introduction

Mass concrete is termed concrete exceeding approximately 0.5 m in the smallest dimension. The combination of low thermal conductivity of concrete with exothermic hydration process and surrounding temperature yields temperature gradients in the concrete mass; consequently significant tensile stresses may develop, leading to early age thermal cracking, which compromise concrete durability (Weiss et al., 1999).

Studies and experience have shown that surface cracking can be minimized or avoided when the maximum differential temperature between the interior and the exterior surface of concrete is limited to less than 20°C (Kosmatka et al., 2003). Besides temperature gradients, the temperature in concrete should not exceed 70°C during hardening to avoid the formation of delayed ettringite accompanied by expansion (Bamforth, 2003).

From the mechanical point of view, the prediction of thermal stresses based on temperature history is a well-established concept. From the material point of view, conversely, predicting temperature evolution due to hydration under adiabatic conditions can be sometimes

[1] Ing. Wilson Ricardo Leal da Silva, Ph.D., Faculty of Civil Engineering, CTU in Prague, Thákurova 7, 166 29 Prague 6, tel. +420 224 35 4629, e-mail: wilsonecv@gmail.com
[2] doc. Ing. Vít Šmilauer, Ph.D., Faculty of Civil Engineering, CTU in Prague, Thákurova 7, 166 29 Prague 6, tel. +420 224 35 4483, e-mail: vit.smilauer@fsv.cvut.cz
[3] doc. Ing. Petr Štemberk, Ph.D., Faculty of Civil Engineering, CTU in Prague, Thákurova 7, 166 29 Prague 6, tel. +420 224 35 4364, e-mail: stemberk@fsv.cvut.cz

complex due to the number of different chemical and physical phenomena involved in cement hydration reactions. Different approaches for modeling hydration reactions are proposed, e.g. CEMHYD3D (Bentz, 2000) and thermo-chemo-mechanical models (Gawin et al., 2006; Hellmich et al., 2001; Ulm and Coussy, 1998). The former is a well-known prediction model that uses a cellular automata approach to simulate microstructure evolution of hydrating cement paste. Whereas the later ones are mainly based on the theory of reactive porous media developed by Coussy (1995).

Although CEMHYD3D has been successfully used in coupled micro/macroscale analysis, the total number of input parameters involved in the calculations is still remarkable (Šmilauer and Krejčí, 2009). As a consequence, this adds too many degrees of freedom for the analysis since several parameters have to be adjusted by the user. Similarly, but to a lower extent, thermo-chemo-mechanical models such as the ones proposed by Gawin et al. (2006), Hellmich et al. (2001), and Ulm and Coussy (1998) also demand a large number of input parameters. Several of these have to be obtained experimentally, thus weakening the model's potential for use by insufficiently skilled personnel.

In that light, and considering practical applications, it is likely that preference is given to hydration models with a few input parameters. In this case, particular attention is put on the model proposed by Cervera et al. (1999). Basically, this consists in a thermo-chemo-mechanical model for concrete, wherein the hydration is modeled based on the chemical affinity of the reactants, i.e. cement and water. More specifically, the hydration reaction is described by a parametric function. The parameters related to such function are adjusted according to the temperature evolution curve of the concrete under adiabatic conditions (Cervera et al., 1999).

The need for adiabatic measurements in practical applications can be troublesome. This is because adiabatic calorimeters are not always available, not to mention their lack of practicality and the costs of acquiring such equipment. To overcome these issues, an experimental setup of a low-cost semi-adiabatic calorimeter is introduced in this work.

The final goal is to use the results from the proposed experimental setup to adjust a hydration model for concrete. The adjusted model is then implemented in FEM analysis to predict the thermal behavior of a mass concrete structure; in particular, a foundation block of a high story building located in Brazil. The results from this analysis are compared against real scale measurements for validation.

2. Heat transport and hydration model

2.1. Weak formulation of heat transport

The transient three dimensional heat conduction problem in incompressible media is derived from a well-known energy balance on a differential element. The combination of this with Fourier's law leads to the differential equation

$$\lambda(\boldsymbol{x})\Delta T(\boldsymbol{x}) + \overline{Q}(\boldsymbol{x},t) = \rho(\boldsymbol{x})c_V(\boldsymbol{x})\frac{\partial T(\boldsymbol{x},t)}{\partial t}, \tag{1}$$

where $T(\boldsymbol{x},t)$ [K] is the unknown temperature field, $\lambda(\boldsymbol{x})$ [Wm^{-1}K^{-1}] is the thermal conductivity of an isotropic material, $\rho(\boldsymbol{x})$ [kg/m^3] stands for a material density, $c_V(\boldsymbol{x})$ [Jkg^{-1}K^{-1}] is a specific heat capacity, and $\overline{Q}(\boldsymbol{x},t)$ [W/m^3] represents a known heat source, in this case, the concrete hydration heat. Initial and boundary conditions can be assigned to Eq. (1).

A weak solution is obtained by multiplying Eq. (1) with a virtual temperature field. After a short elaboration, a weak formulation reads

$$\mathbf{C}\dot{\boldsymbol{r}} + \mathbf{K}\boldsymbol{r} = \boldsymbol{p}, \tag{2}$$

$$\mathbf{K} = \int_{\Omega} \mathbf{B}(\boldsymbol{x})^T \lambda(\boldsymbol{x}) \mathbf{B}(\boldsymbol{x}) \mathrm{d}\Omega, \tag{3}$$

$$\mathbf{C} = \int_{\Omega} \mathbf{N}(\boldsymbol{x})^T \rho(\boldsymbol{x}) c_V(\boldsymbol{x}) \mathbf{N}(\boldsymbol{x}) \mathrm{d}\Omega, \tag{4}$$

$$\boldsymbol{p} = -\int_{\Gamma_{c,T,\overline{q}}} \mathbf{N}(\boldsymbol{x})^T \boldsymbol{n}(\boldsymbol{x})^T \boldsymbol{q}(\boldsymbol{x},t) \mathrm{d}\Gamma + \int_{\Omega} \mathbf{N}(\boldsymbol{x})^T \overline{Q}(\boldsymbol{x},t) \mathrm{d}\Omega, \tag{5}$$

where $\mathbf{K}$ is the conductivity matrix, $\mathbf{C}$ is the capacity matrix, and ($\boldsymbol{p}$) is the heat load vector, which captures both the boundary conditions and the heat source. All temperature-dependent terms will appear on the left hand side of Eq. (2). A v-form version of the trapezoidal scheme is used for solution in the form of predictor-corrector (Hughes, 2000).

2.2. Affinity hydration model

Affinity hydration models provide a framework for accommodating all stages of cement hydration. Consider hydrating cement under isothermal temperature 25°C. At this temperature, the rate of hydration can be expressed by the chemical affinity $\widetilde{A}_{25}(DoH)$ as

$$\frac{\mathrm{d}DoH}{\mathrm{d}t} = \widetilde{A}_{25}(DoH), \tag{6}$$

where the chemical affinity has a dimension of time^{-1}. The affinity for isothermal temperature can be obtained experimentally; in particular, isothermal calorimetry measures a heat flow $q(t)$ which gives the hydration heat $Q(t)$ after integration.

Cervera et al. (1999) proposed an analytical form of the normalized affinity, which was further refined by Gawin et al. (2006). A slightly modified formulation is proposed in this work

$$\frac{\mathrm{d}DoH}{\mathrm{d}t} = \widetilde{A}_{25}(DoH) = B_1 \left(\frac{B_2}{DoH_\infty} + DoH \right) (DoH_\infty - DoH) \exp\left(-\bar{\eta} \frac{DoH}{DoH_\infty} \right), \tag{7}$$

where B_1 and B_2 are coefficients to be adjusted, DoH_∞ is the ultimate hydration degree, and $\bar{\eta}$ represents the micro-diffusion of free water through formed hydrates. The parameters from Eq. (7), i.e. B_1, B_2, DoH_∞, and $\bar{\eta}$, express isothermal hydration at 25°C. When hydration proceeds under varying internal temperature, which is the case of adiabatic conditions, the affinity $\widetilde{A}_{25}(DoH)$ is scaled via Arrhenius equation to arbitrary temperature T

$$\widetilde{A}_T = \widetilde{A}_{25} . \exp\left[\frac{E_a}{R} . \left(\frac{1}{273.15 + 25} - \frac{1}{T} \right) \right]. \tag{8}$$

For example, simulating isothermal hydration at 35°C means scaling $\widetilde{A}_{25}$ with a factor of 1.651 at a given time. This means that hydrating concrete for 10 hours at 35°C releases the same amount of heat as concrete hydrating for 16.51 hours under 25°C. Notice that setting E_a= 0 in Eq. (8) ignores the effect of temperature and proceeds the hydration under 25°C. Fig. 1 validates the presented parametric affinity model on a w/c = 0.5 OPC "Mokra". Particularly, the parameters from Eq. (7) were fitted to B_1= 1.2667 h^{-1}, B_2= 8.0e-6, $\bar{\eta}$= 7.4, and DoH_∞= 0.85.

The multiscale model, implementing structural scale and affinity hydration model, was implemented in OOFEM package, which may be freely downloaded and used (Patzák et al., 1993).

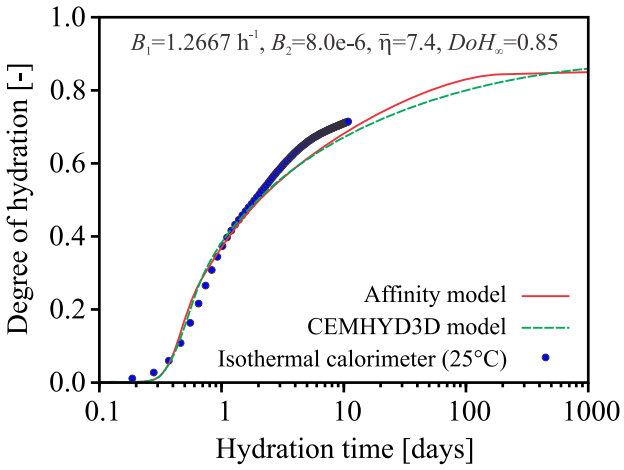

Fig. 1: Validation of the affinity model on OPC with a $w/c = 0.5$.

3. Experimental program

The experimental program proceeded from a small semi-adiabatic calorimeter to a large foundation block. The results from the numerical simulation are presented in section 4.

3.1. Semi-adiabatic calorimeter

The semi-adiabatic experimental setup consists of a concrete cube with an edge of 240 mm covered by a 100 mm thick polystyrene foam. The temperature measurements are based on K-type thermocouples, and the measured data are collected by a datalogger (Pico Log TC-08). The configuration of the proposed experimental setup is illustrated in Fig. 2. The concrete composition C1, which is detailed in Table 1, was monitored in the semi-adiabatic calorimeter.

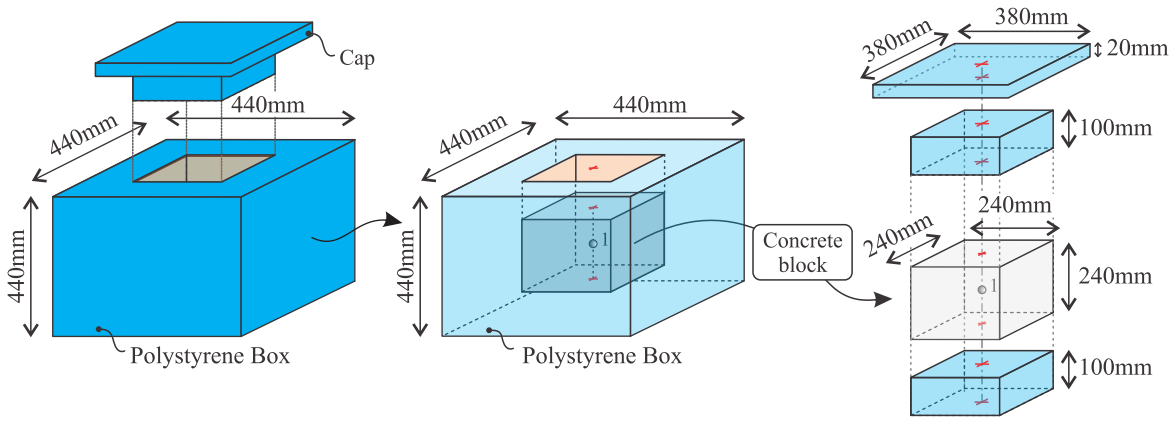

Fig. 2: Semi-adiabatic experimental setup.

3.2. Mass concrete foundation block

The foundation block of a residential building with 35 floors is located in Balneario Camboriu, Brazil. The block has the dimensions of $19.6 \times 10.1 \times 2.5$ m. At the end, 511.0 m^3 of concrete

Tab. 1: Composition of concrete mixtures C1 and C2.

	Composition [kg/m^3]	
Materials	C1	C2
Cement CP IV RS[(1)]	420	408
River Sand (S)	750	720
Coarse Aggregate 1 (Max. grain size: 12.5 mm)	1020	255
Coarse Aggregate 2 (Max. grain size: 25.0 mm)	-	765
Water	138.6	140.7
Crushed ice	59.4	60.3
Water reducing admixture[(2)]	0.65%	0.65%
High range water reducing admixture[(2)]	0.44%	0.32%

[(1)] The physicochemical characterization is shown in NBR5736 (1991).
[(2)] Percent of cement mass.

was cast. The details of the formwork, gravel bed, and dimensions of the block are shown in Fig. 3.

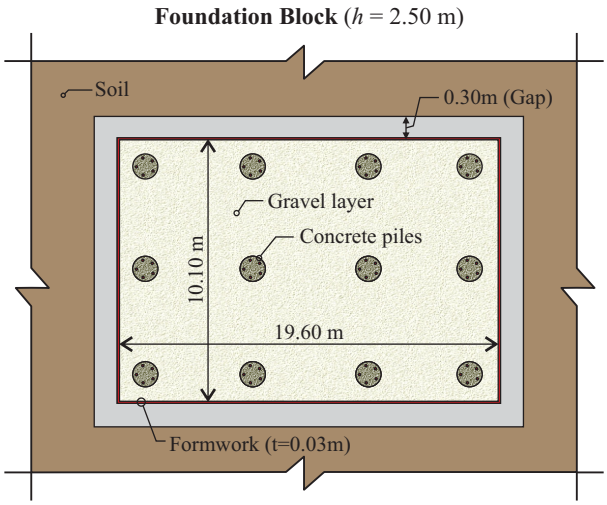

Fig. 3: Details of the evaluated foundation block.

To avoid working joints between concrete layers, continuous casting of concrete was performed by concrete pumps for about twelve hours. Two concrete mixtures, namely C1 and C2, were used in the foundation block. Their compositions are listed in Table 1.

From Table 1 it can be noticed that C1 and C2 are slightly different. The main difference between them is the maximum size of coarse aggregates. Reduced maximum size of aggregates in C1 was necessary because of the heavily reinforced areas located at the bottom of the block. C2 was poured in the block after the reinforcement at the bottom layer was completely covered. Since C1 and C2 are nearly the same concerning cement content, it is reasonable to assume that the concrete block is composed of an unique mixture, which was assumed to be C1.

After block casting, the concrete surface that was exposed to the ambient was flooded with a layer of water to assure adequate curing. Such technique, known as ponding or flooding, allows for reducing loss of moisture on concrete surface, thus preventing cracking at early ages. Additionally, it reduces the heat transfer between concrete and the ambient air, leading to a

slower cooling process when combined with insulation systems (Neville, 1997).

4. Results and discussion

The thermal conductivity of concrete was assumed to be constant and equals to 1.8 $Wm^{-1}K^{-1}$ during all simulations. This value is quite common in structural concretes as found in investigations, e.g. Kim et al. (2003) and Guo et al. (2011). Although thermal conductivity slightly decreases when concrete binds more capillary water into hydration products Faria et al. (2006), its value was considered constant in this anaylsis.

The heat capacity of concrete was adopted to be equal to 870 $Jkg^{-1}K^{-1}$ during all simulations. It is known from concrete science that heat capacity does not change significantly during concrete hardening and the use of a constant value is a reasonable assumption (Choktaweekarn and Tangtermsirikul, 2010).

Both simulations assumed the same concrete composition C1 according to Table 1. Clinker composition of cement yielded 518.37 J/g but the cement used was blended. It turned out from the simulations that 45% of cement needs to be replaced by any inreactive material (fly ash + slag) used as a supplementary cementitious material. The contribution of slag and fly ash is insignificant for first days of hydration (Šmilauer, 2013). The effective amount of clinker is therefore $0.55 \cdot 420 = 230\,kg/m^3$ of concrete. This value was used in all simulations.

Hydration kinetics of cement was calibrated from semi-adiabatic experiment. The parameters according to Eqs.(7) and (8) were fitted to $B_1 = 0.0007\ s^{-1}$, $B_2 = 6.0e\text{-}5$, $\eta = 6.1$, $DoH_\infty = 0.85$, and $E_a = 38.3$ kJ/mol.

4.1. Semi-adiabatic calorimeter

Fig. 4a shows the calibration of the multiscale model and indicates that the hydration kinetics was fitted quite reasonably. The maximum temperature in the middle of the cube reached 55.2°C after 16 hours of hydration. Fig. 4b displays the corresponding temperature field for a quarter of the cube.

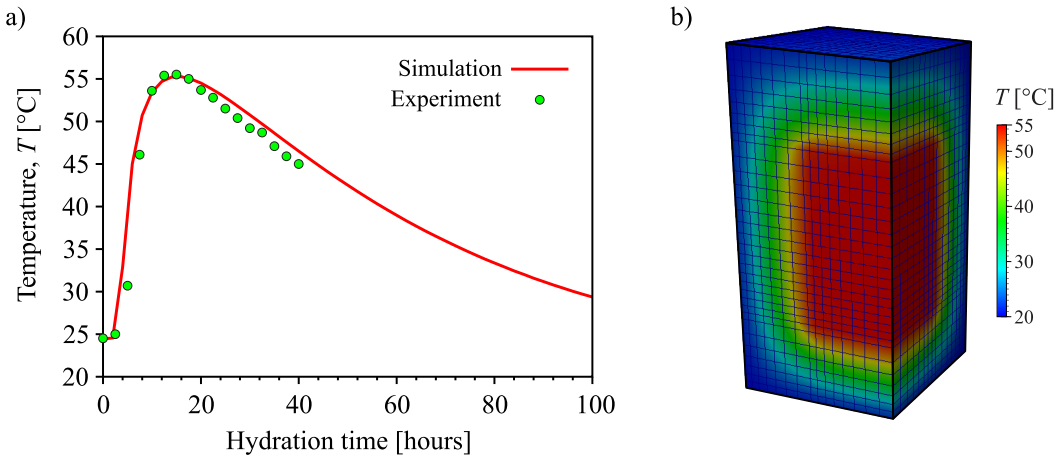

Fig. 4: Semi-adiabatic calorimeter: a) calibration of the multiscale model from the semi-adiabatic calorimeter and b) temperature field during maximum core temperature.

4.2. Mass concrete foundation block

The mass concrete foundation block has the dimensions of $19.6 \times 10.1 \times 2.5$ m. Fig. 5 shows such details about geometry, mesh, boundary conditions, and control temperature points in the foundation block. Notice that, due to symmetry conditions, only a fourth of the block was modeled. Also, although the block was continuously cast for a period of ≈12 hours, two concrete layers with time offset of 6 hours were considered in the analysis. This led to a better temperature agreement in the upper layers of the block.

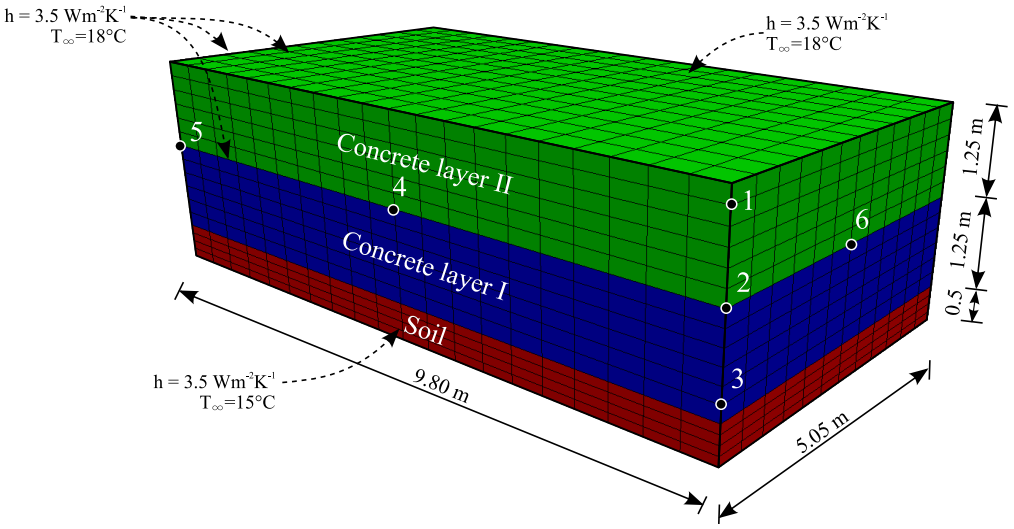

Fig. 5: Geometry, mesh, boundary conditions, and control temperature points (temperature gauges) in the mass concrete foundation block.

In addition, a few other things turned out during the model built-up. First, the soil thermal capacity had to be taken into account to avoid the observation of temperature mismatch in the temperature gauge 3. Particularly, soil density of 2000 kg/m^3, thermal conductivity of 0.8 Wm^{-1}K^{-1}, and heat capacity of 840 Jkg^{-1}K^{-1} were assumed. Second, the temperature fluctuation at the top of concrete block was disregarded, which is visible in the measurements from temperature gauge 1 in Fig. 6.

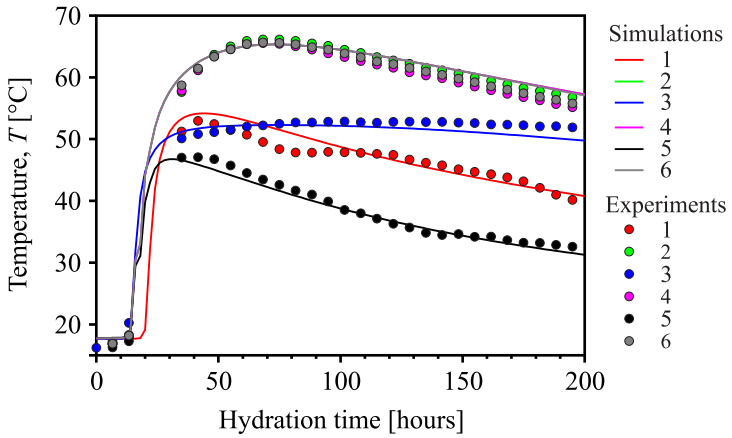

Fig. 6: Temperature evolution in temperature gauges and results from the simulation.

The initial temperature of soil and both concrete layers was set up to 17.7°C. The same concrete composition C1 according to Table 1 was assumed. In total, 3840 brick finite elements with 4641 nodes created the geometry. The integration time step was set to 2 hours and 100 steps were executed. The computation ran for 10 minutes in OOFEM (Patzák et al., 1993).

Fig. 6 validates temperature evolution in the block. Inner gauges 2, 4, and 6 gave practically the same temperature evolution, which was slightly influenced by boundary conditions. The maximum temperature in gauges 2, 4, and 6 reached 65°C at 74 hours of hydration. Fig. 7 shows the corresponding temperature field and testifies that the soil temperature below the block raised up.

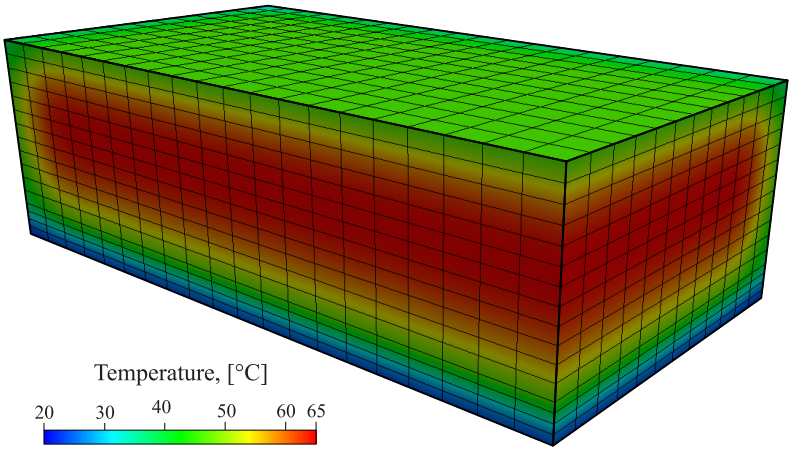

Fig. 7: Temperature field at 74 hours.

To sum up, the six gauges that were placed in the mass concrete foundation block gave the global overview of temperatures in the block and validated the multiscale model for concrete hydration.

5. Conclusion

A unique set of experimental data proved that calibrating an affinity hydration model to a small-size concrete cube under semi-adiabatic conditions can be applied to a large-scale block with different boundary conditions. Hence, the proposed experimental setup can be a suitable alternative to the standard adiabatic calorimeter. This solution turns out to be highly attractive for the concrete industry due to its low cost.

The methodology that was used to simulate concrete thermal behavior indicates that proper mathematical formulation and a suitable affinity model for hydrating concrete can be applicable to any shape and size of hydrating concrete. Also, the upscaling of small laboratory experiments to large-scale massive structures has several advantages over traditional empirical methods. For example, it enables time-efficient simulation and selection of a suitable concrete mix.

Currently, a graphical and semi-automatic tool is being developed for the concrete industry with the same objectives and methodology.

6. Acknowledgment

The financial support from Czech Science Foundation grant No. 105/10/2400 and from Grant Agency of the CTU in Prague SGS12/116/OHK1/2T/11 and SGS13/039/OHK1/1T/11 are gratefully acknowledged.

7. References

Bamforth, P. (2003) Concreting large-volume (mass) pours, In: Newman, J., Choo, B.S., Choo, B.S., editors. *Advanced Concrete Technology Set*. Oxford, Butterworth-Heinemann, pp.1-47.

Bentz, D. (2000) *A three-dimensional cement hydration and microstructure development modeling package*, Technical Report Version 3.0, NIST Building and Fire Research Laboratory, Gaithersburg, MD.

Brazilian Association of Technical Standards (1991) NBR 5736: Pozzolanic Portland cement - Specification, Rio de Janeiro, Brazil.

Cervera, M., Oliver, J., Prato, T. (1999) Thermo-chemo-mechanical model for concrete. I: Hydration and aging, *Journal of Engineering Mechanics ASCE*, 125, 9, pp.1018-1027.

Choktaweekarn, P., Tangtermsirikul, S. (2011) Effect of aggregate type, casting, thickness and curing condition on restrained strain of mass concrete, *Songklanakarin Journal of Science and Technology*, 32, pp.391-402.

Coussy, O. (1995) *Mechanics of Porous Media*. New York, Wiley.

Faria, R., Azenha, M., Figueiras, J.A. (2006) Modelling of concrete at early ages: Application to an externally restrained slab, *Cement and Concrete Composites*, 28, 6, pp.572-585.

Gawin, D., Pesavento, F., Schrefler, B.A. (2006) Hygro-thermo-chemo-mechanical modelling of concrete at early ages and beyond. Part I: Hydration and hygro-thermal phenomena, *International Journal for Numerical Methods in Engineering*, 67, 3, pp.299-331.

Guo, L., Guo, L., Zhong, L., Zhu, Y. (2011) Thermal conductivity and heat transfer coefficient of concrete, *Journal of Wuhan University of Technology (Material Science Edition)*, 26, pp.791-796.

Hellmich, C., Mang, H.A., Ulm, F.J. (2001) Hybrid method for quantification of stress states in shotcrete tunnel shells: combination of 3D in situ displacement measurements and thermochemoplastic material law, *Computers & Structures* , 79, 22-25, pp.2103-2115.

Hughes, T.J.R.. *The Finite Element Method: Linear Static and Dynamic Finite Element Analysis*, Dover Publications; 2000.

Kim, K.H., Jeon, S.E., Kim, J.K., Yang, S. (2003) An experimental study on thermal conductivity of concrete, *Cement and Concrete Research*, 33, 3, pp.363-371.

Kosmatka, S., Kerkhoff, B., Panarese, W. (2003) *Design and Control of Concrete Mixtures*, 14th ed., Portland Cement Association.

Neville, A.M. (1997) *Properties of Concrete*, 4th ed., London, Wiley.

Patzák, B., et al., (1993) Object Oriented Finite Element Method - OOFEM. Available at http://www.oofem.org.

Šmilauer, V., Krejčí, T. (2009) Multiscale model for temperature distribution in hydrating concrete *International Journal for Multiscale Computational Engineering*, 7, 2, pp.135-151.

Šmilauer, V. (2013) *Multiscale hierarchical modeling of hydrating concrete*, Saxe-Coburg Publications.

Ulm, F.J., Coussy, O. (1998) Couplings in early-age concrete: From material modeling to structural design. *International Journal of Solids and Structures*, 35, 31-32, pp.4295-4311.

Weiss, W., Yang, W., Shah, S. (1999) Factors influencing durability and early-age cracking in high strength concrete structures, In: *High Performance Concrete: Research to Practice*. Farmington Hills, MI, SP 189-22, pp.387-409.